

## Small-Angle Scattering Observed in the Formation of Neutral Atoms from 10- to 55-keV Positive Ion Beams

A. B. WITTKOWER, P. H. ROSE, R. P. BASTIDE, AND N. B. BROOKS

Research Tandem Group, High Voltage Engineering Corporation, Burlington, Massachusetts

(Received 6 July 1964)

Beams of  $H^+$ ,  $D^+$ ,  $He^+$ , and  $N^+$  from 10–55 keV were passed through a small aperture at the entrance of a charge-changing gas target, where neutral atoms were formed by electron attachment. The attachment scattering was measured by scanning the neutral beam beyond the target cell. The increase in beam diameter was measured as a function of the target thickness. It was found that the scattering approximated a normal distribution, and the half-width at half-maximum was used to describe the attachment scattering angle. This angle, which was about one milliradian, was measured as a function of the energy and target thickness for a number of scattering gases.

### INTRODUCTION

THE large-angle attachment scattering angle has recently been studied intensively by Everhart and his co-workers.<sup>1</sup> They have found that at low energies (<50 keV) and for projectiles of low atomic number, essentially all the neutral atoms formed in the attachment process are contained within an angle<sup>2</sup> of  $1^\circ$ . Specifically, Everhart has chosen to work with those few neutral atoms observed at larger angles. The small-angle scattering has previously been studied by Johnson,<sup>3</sup> but in an experiment which gave a distorted picture in certain important respects. In the experiment reported below, this source of error has been removed. The attachment scattering of  $H^+$ ,  $D^+$ ,  $He^+$ , and  $N^+$  beams in  $H_2$ , He,  $N_2$ ,  $O_2$ , Ne, and Ar gases has been studied as a function of target thickness and beam energy (10–55 keV).

### APPARATUS

The apparatus is shown in Fig. 1. Positive ions are accelerated to their final energy by extraction from an rf ion source. Both the probe voltage supply, which was always set at +5 kV, and the extraction voltage supply

were voltage-regulated to <0.1% ripple. The beam was momentum-analyzed by a  $20^\circ$  magnet powered by a supply, the current ripple of which was also <0.1%. The ions left the source in a divergent beam, and no focusing of this beam was attempted, other than that inadvertently achieved by the  $20^\circ$  magnet. The beam, therefore still divergent, passed through a 0.25-mm hole at the entrance of the scattering chamber. The scattering chamber, which was differentially pumped as shown in the figure, was constructed so that scattered beam could leave the chamber at all angles less than  $\pm 25$  mrad. Scattering gas was admitted in a high-conductance region immediately behind the entrance aperture, and the cell pressure was read by a Pirani gauge at this point. Beyond this high-conductance region, the cell was made in the form of a divergent slot 0.635 cm in one dimension, and diverging from 0.09 to 0.635 cm in the other dimension. This allowed the divergence to be maintained at  $\pm 25$  mrad while reducing the conductance of the exit section. Beyond the cell, the beam entered a differentially pumped section maintained at a low pressure,  $<4 \times 10^{-6}$  Torr at the maximum target thickness. Calculations show that <0.5% of the total target thickness was outside the cell region. At a

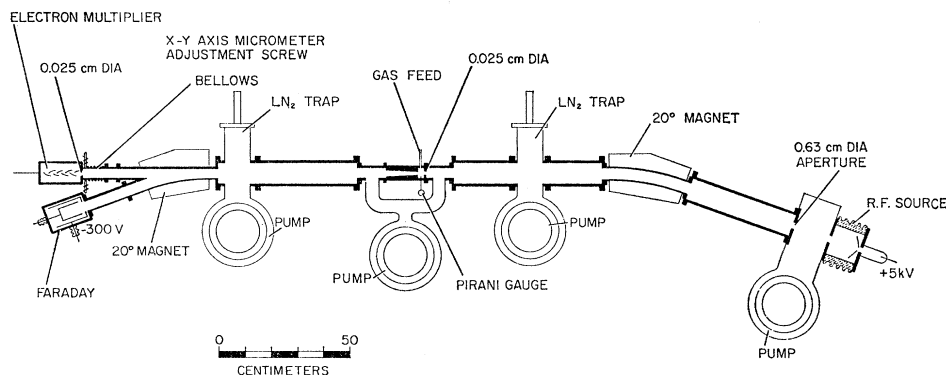


FIG. 1. A schematic diagram of the experimental apparatus.

<sup>1</sup> A few representative references are: E. Everhart, R. J. Carbone, and G. Stone, *Phys. Rev.* **98**, 1045 (1955); F. P. Ziemba, G. J. Lockwood, G. H. Morgan, and E. Everhart, *ibid.* **118**, 1552 (1960); G. J. Lockwood, H. F. Helbig, and E. Everhart, *ibid.* **132**, 2078 (1963).

<sup>2</sup> P. R. Jones, F. P. Ziemba, H. A. Moses, and E. Everhart, *Phys. Rev.* **113**, 182 (1959).

<sup>3</sup> B. L. Johnson, *J. Appl. Phys.* **33**, 739 (1962).

second 20° analyzing magnet, charged components of the beam were removed from the neutral fraction and could be measured in a biased Faraday cup. The neutral beam continued through this magnet undeflected, and was scanned by a second 0.25-mm hole which was moved across the beam diameter by a micrometer screw. Neutral atoms passing through the hole and causing secondary emission were detected by observing the dc current at the collector of an electron multiplier with an electrometer. The output of the electrometer was attached to the y sweep of an x-y recorder, while the x sweep was generated by the voltage from a linear potentiometer attached to the 0.25-mm aperture-plate holder. In this way the intensity profile of the neutral beam across its diameter was recorded for various values of beam energy and target thickness.

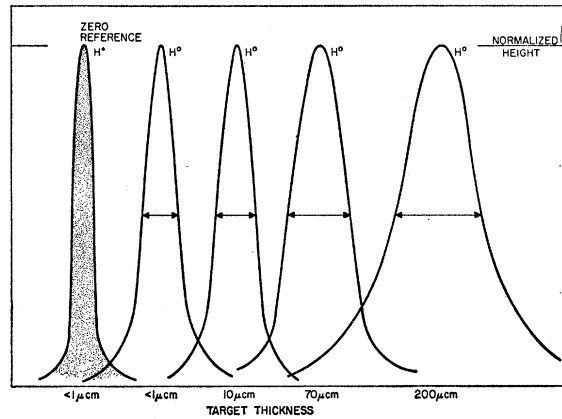


FIG. 2. Typical intensity profiles of the neutral beam at the detector as a function of target thickness. The intensity profile of the unscattered positive-ion beam is shown on the left.

FIG. 3. The attachment scattering half-angle of  $H^+$  ions at 30 keV in  $H_2$  gas versus target thickness. In the insert, data taken at a proton energy of 55 keV show an expansion of the region about the origin. It can be seen that the attachment scattering half-angle is independent of the target thickness.

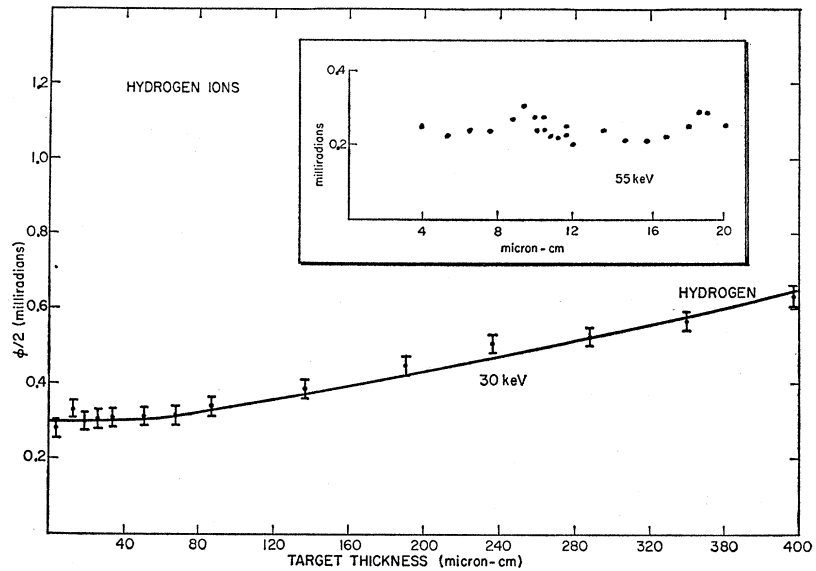
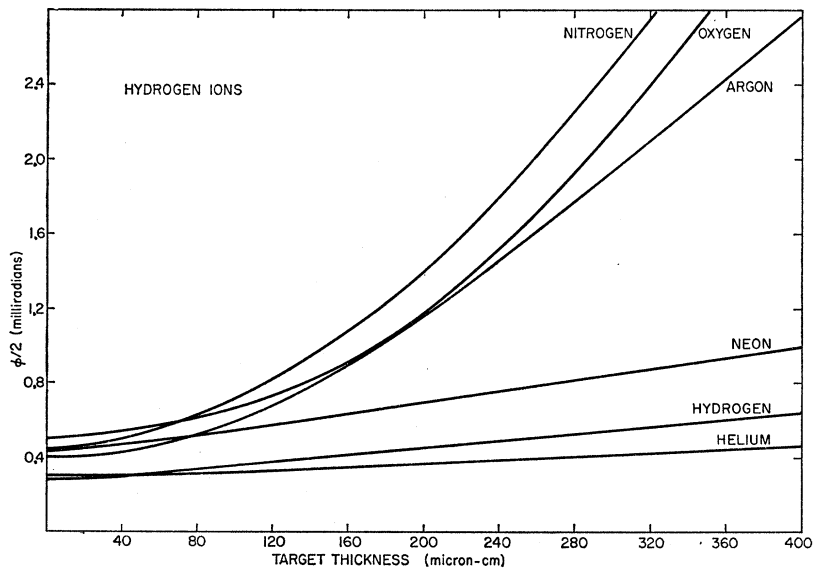


FIG. 4. The attachment scattering half-angle of  $H^+$  ions at 30 keV in a variety of target gases versus target thickness.



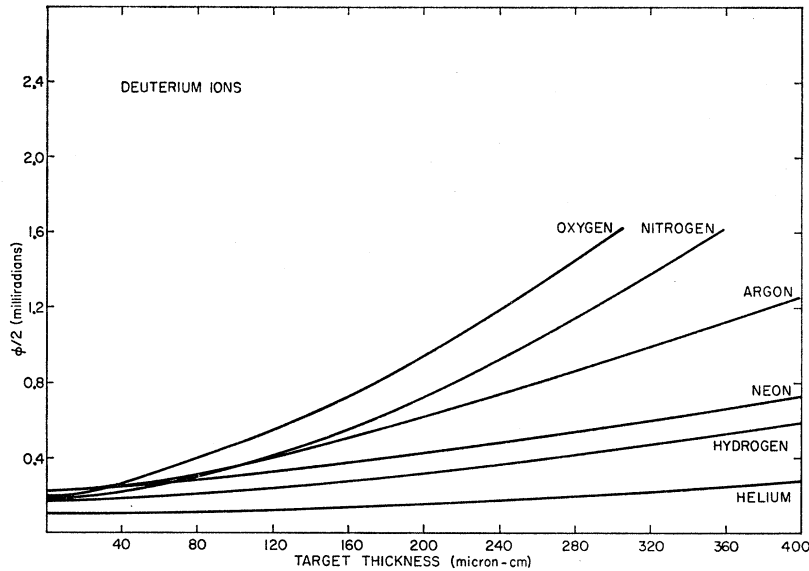


FIG. 5. The attachment scattering half-angle of  $D^+$  ions at 30 keV in a variety of target gases versus target thickness.

#### EXPERIMENTAL DETAILS

##### Measurement of Scattering Angle

The apparatus described above adequately measures the increase in scattering angle with target thickness. However, in order to obtain a "zero reference angle," it is essential to measure the minimum width of the beam when no scattering whatsoever occurred. This measurement was achieved by scanning the width of the initial positive ion beam with no gas in the cell and the second analyzing magnet switched off. It was the ability to make this measurement which distinguished these results from those of Johnson. Typical intensity profiles are shown in Fig. 2. The "zero reference" or inherent geometrical width of the system is illustrated by a scan across the positive ion beam. In subsequent

profiles at increasing target thicknesses, the width of the neutral beam is shown. It can be seen that even at the lowest target thickness there is an appreciable increase in the width of the neutral-beam profile  $w_f$  over the "zero-reference" width  $w_+$ . As the center portion of each profile appeared to have a near-Gaussian distribution over at least two half-widths, the measurement of each profile was made in terms of the half-width at half-maximum. In order to assess the increase in width due to scattering  $w_0$ , the zero-reference half-width  $w_+$  was subtracted from the final half-width  $w_f$  as follows:

$$w_0 = (w_f^2 - w_+^2)^{1/2}.$$

The scattering half-angle  $\frac{1}{2}\phi$  quoted in the results was then

$$\frac{1}{2}\phi = w_0/2d,$$

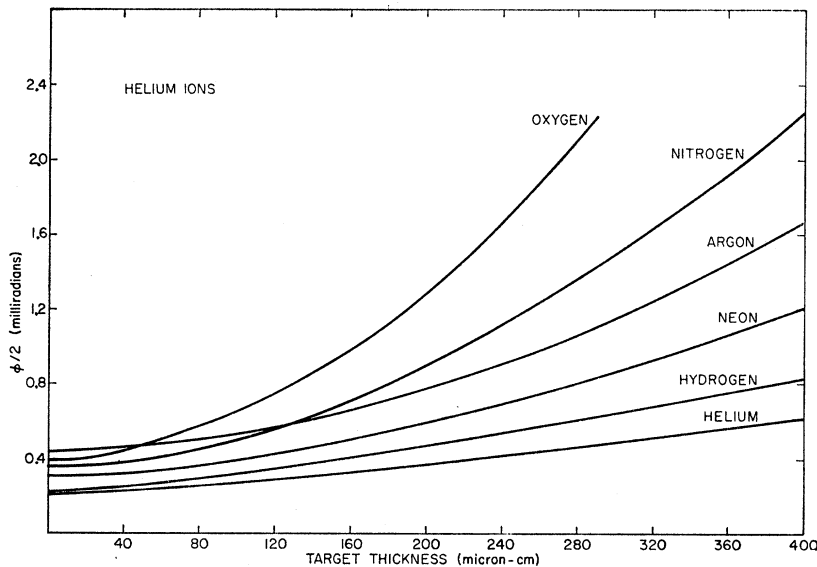
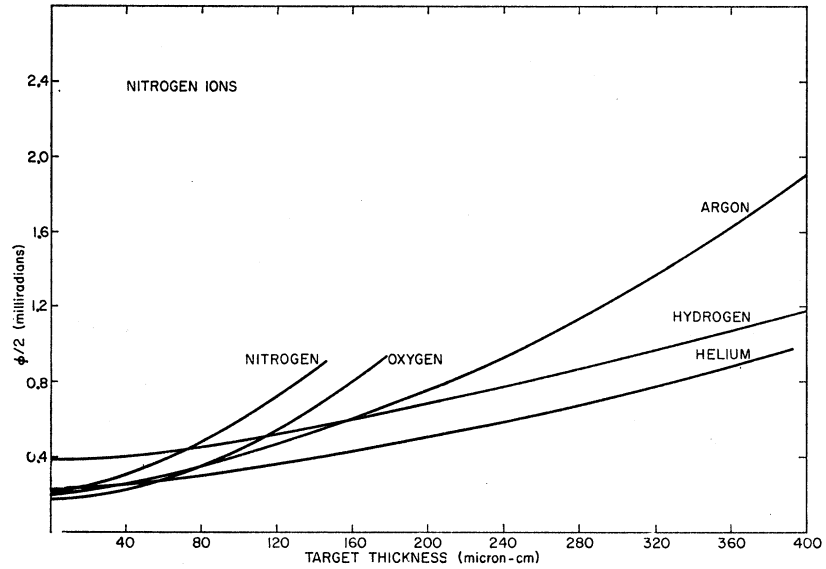


FIG. 6. The attachment scattering half-angle of  $He^+$  ions at 30 keV in a variety of target gases versus target thickness.

FIG. 7. The attachment scattering half-angle of  $N^+$  ions at 30 keV in a variety of target gases versus target thickness.



where  $d$  is the distance between the scattering cell and the detector aperture. It is apparent that 50% of the neutral particles are contained within the scattering angle  $\phi$ , if the distribution of particles is truly Gaussian.

**Measurement of Target Thickness**

The target thickness was measured by a Pirani gauge located in the high-conductance section of the gas cell. By integration, the pressure distribution along the length of the cell was calculated, and the target thickness was determined to be  $4.0 P \mu\text{-cm}$ , where  $P$  is the cell pressure in microns. The Pirani gauge was calibrated for each of the scattering gases against a McLeod gauge.

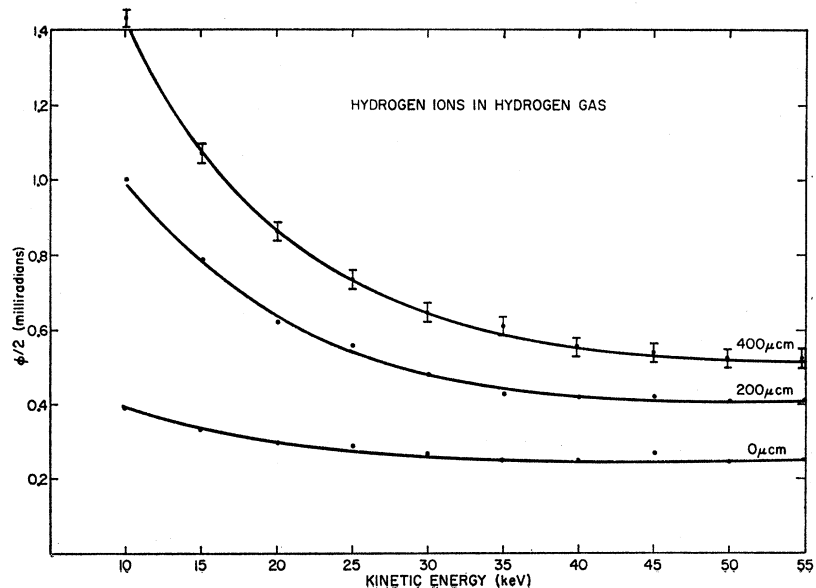
**RESULTS**

The attachment scattering of  $H^+$ ,  $D^+$ ,  $He^+$ , and  $N^+$  at 30 keV in gases is shown in Figs. 3-7. In Figs. 8-10, the attachment scattering of  $H^+$  ions in  $H_2$ , He, and Ar gases is shown as a function of beam energy for various target thicknesses.

**DISCUSSION**

In order to discuss the form of the results specifically, the attachment scattering of  $H^+$  in  $H_2$  gas will be considered (see Figs. 3, 4, and 8). In Fig. 3, it can be seen that, after an initial step at the  $y$  axis, the scattering increases with increasing target thickness, as might be expected. Experimental points are shown on this figure,

FIG. 8. The attachment scattering half-angle of  $H^+$  ions in  $H_2$  gas as a function of the ion energy.



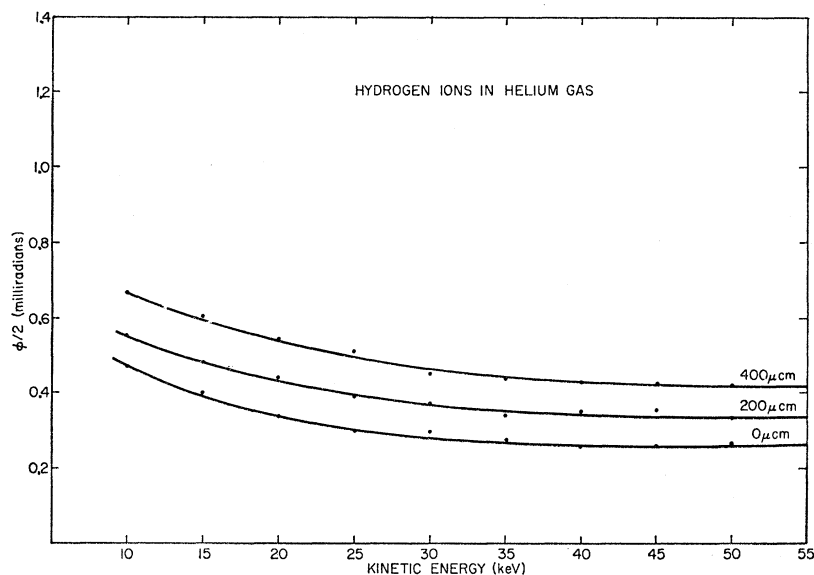


FIG. 9. The attachment scattering half-angle of  $\text{H}^+$  ions in He gas as a function of the ion energy.

and the error bars are typical of all the measurements. At an extremely thin target thickness, it is very probable that almost every proton will pass through the cell without interacting in any way with the target gas. Therefore, it is extremely unlikely that any proton which has been able to attach an electron has any other interaction within the cell. Verification of this statement is shown in the insert of Fig. 3; it can be seen that near the origin, the scattering angle does not rise with increasing target thickness, indicating a single-interaction scattering process. The fact that there is an observable scattering angle at the lowest thicknesses can therefore be related directly to the attachment of the electron. However, even in this case, several "exit channels" exist as both the fast atom and the residual

ion may leave the interaction in one of many excited states or in the ground state, and no specific interpretation about the height of the step can be made at present. As the target thickness increases, it becomes more probable that plural charge changes will occur as well as elastic or inelastic collisions without an additional charge change. Cross sections for some of these reactions have either been calculated (for H ions or atoms in atomic hydrogen gas) or measured (for H ions in molecular hydrogen gas), and values are shown in Table I. In Fig. 11, a histogram has been plotted showing the probability for  $n$ -charge changes at 100  $\mu\text{-cm}$  target thickness for  $\text{H}^+$  ions at 30 keV charge-changing in  $\text{H}_2$  gas. This region is therefore extremely complicated, as the scattering angle depends upon the inter-

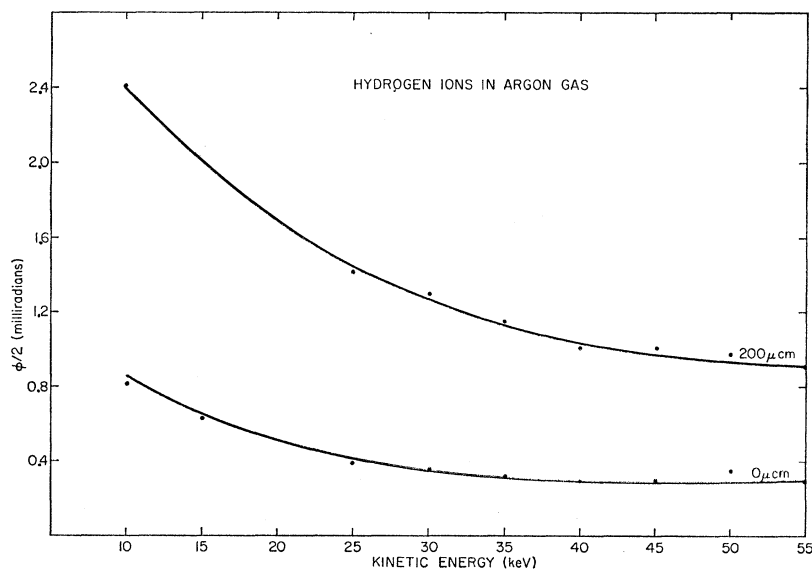


FIG. 10. The attachment scattering half-angle of  $\text{H}^+$  ions in Ar gas as a function of the ion energy.

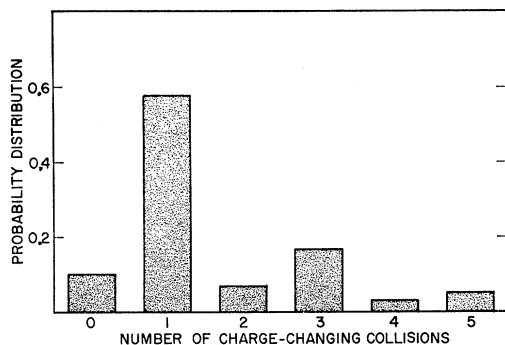


FIG. 11. The calculated probability distribution that a given number of charge-changing collisions will occur for  $H^+$  ions at 30 keV passing through a target of  $H_2$  gas with a target thickness of  $100 \mu\text{-cm}$ . The fact that the cross section for the production of neutral atoms from protons,  $\sigma_{10}$ , is greater than the cross section for the inverse reaction,  $\sigma_{01}$ , increases the probability for an odd number of charge changes.

play of all the cross sections. At highest target thickness, and looking now at all the curves in Fig. 4, the attachment scattering angle can be seen to depend upon the scattering material. However, rather than increasing as the charge or mass of the scattering gas, as would be expected from classical theory, it can be seen in Table II that the scattering angle at large target thickness is closely related to the molecular area. Although it has been well established in the past that the charge-changing cross sections depend upon the molecular area, it was the somewhat unexpected result of these experiments that the attachment scattering also follows a similar trend.

TABLE I. Cross sections in  $\text{cm}^2/\text{atoms}$  for certain related reactions.

	10 keV	30 keV	50 keV	Multiplier
Attachment $\sigma_{10}^{a,d}$	3.99	2.10	0.90	$10^{-16}$
Loss $\sigma_{01}^{a,d}$	0.44	0.80	0.78	$10^{-16}$
$\sigma$ for secondary $H_2^+$ by $H^+$ impact <sup>b,d</sup>	4.6	2.70	1.80	$10^{-16}$
$\sigma$ for secondary $H^+$ by $H^+$ impact <sup>b,d</sup>	1.7	1.50	0.80	$10^{-16}$
$\sigma$ for free electrons in $H_2$ gas by $H^{+b,d}$	0.45	0.90	1.30	$10^{-16}$
Ionization by $H^+$ impact <sup>c,e</sup>	4.50	4.50	4.00	$10^{-17}$
Ionization by $H^+$ impact <sup>c,e</sup>	2.0	2.00	1.90	$10^{-16}$
Excitation $\sigma$ by $H^+$ impact <sup>c,e</sup> : $\left\{ \begin{array}{l} 2s \\ 2p \end{array} \right.$	7.0	2.00	1.20	$10^{-18}$
From ground state to $\left\{ \begin{array}{l} 2p \\ 3p \end{array} \right.$	14.0	5.00	3.20	$10^{-18}$
Excitation $\sigma$ by $H^+$ impact <sup>c,e</sup> : $\left\{ \begin{array}{l} 2s \\ 2p \end{array} \right.$	3.0	1.30	0.90	$10^{-18}$
From ground state to $\left\{ \begin{array}{l} 2p \\ 3p \end{array} \right.$	16.0	15.0	14.0	$10^{-17}$
	2.80	2.80	2.40	$10^{-17}$

<sup>a</sup> P. M. Stier and C. F. Barnett, Phys. Rev. **103**, 896 (1956).  
<sup>b</sup> V. V. Afosimov, R. N. Il'in, and N. V. Fedorenko, Sov. Phys-JETP **7**, 968 (1958).

<sup>c</sup> D. R. Bates and D. W. Griffing, Proc. Phys. Soc. (London) **A66**, 961 (1953).

<sup>d</sup> Experimental determining in  $H_2$  gas.

<sup>e</sup> Theoretical calculation in atomic hydrogen.

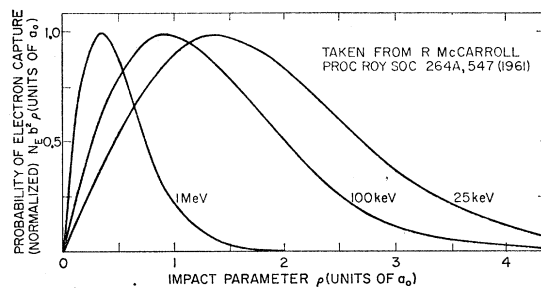


FIG. 12. The probability of electron capture versus the impact parameter for a number of proton energies.

In Fig. 8, the attachment scattering is seen to decrease with increasing beam energy, as might be expected, at least at the lower energies. However, above 30 keV, the decrease in scattering angle is not appreciable and the curve tends to level off. The existence of this plateau, particularly in the extrapolated curve  $t=0 \mu\text{cm}$ , is inexplicable unless more momentum is transferred in the attachment process at the higher energies than at the lower energies. An indication that this phenomenon is likely to occur has been given by McCarroll,<sup>4</sup> from whose paper Fig. 12 has been taken.

TABLE II. Attachment scattering of ions in gases (target thickness  $300 \mu\text{cm}$ ) at 30 keV.

Attachment gas	$H_2$	He	$N_2$	$O_2$	Ne	Ar
Molecular area <sup>a</sup> $\times 10^{-16} \text{cm}^2$	5.6	3.8	11.1	10.3	5.3	10.5
Ion species	$H_1^+$	$He^+$	$N_2^+$	$O_2^+$	Ne	Ar
$\frac{1}{2}\phi$ at 300 $\mu\text{cm}$ (milliradians)	0.54	0.42	2.50	2.17	0.84	1.94
	0.44	0.22	1.26	1.58	0.57	0.92
	0.65	0.52	1.50	2.12	0.87	1.14
	0.91	0.72	$>O_2$	$<N_2$	...	1.24

<sup>a</sup> Values from E. W. McDaniel, *Collision Phenomena in Ionized Gases* (John Wiley & Sons, Inc., New York, 1964).

In this figure it is shown that the most probable impact parameter for electron capture decreases as the beam energy increases. The probability of a more violent collision imparting an increased momentum to the fast particle is therefore more likely at the higher energies.

Finally, it must be pointed out that the rather large scattering angles observed by the attachment scattering of the heavier ions  $He^+$  and  $N^+$  in gases is not understood. On the basis of classical dynamics, a  $N^+$  ion at 30 keV would be scattered at a smaller angle than a  $H^+$  ion of the same energy, if the interaction momentum interchange were the same in both cases.

<sup>4</sup> R. McCarroll, Proc. Roy. Soc. (London) **A264**, 547 (1961).